Revealing Ion Adsorption and Charging Mechanisms in Layered Metal-Organic Framework Supercapacitors with Solid-State Nuclear Magnetic Resonance

Chloe J. Balhatchet[1], Jamie W. Gittins[1], Seung-Jae Shin[2], Kangkang Ge[3], Xinyu Liu[1], Teedhat Trisukhon[1], Shivani Sharma[1,4], Thomas Kress[1], Pierre-Louis Taberna[3,5], Patrice Simon[3,5], Aron Walsh[2], Alexander C. Forse[1*]

[1] Yusuf Hamied Department of Chemistry, University of Cambridge, Lensfield Road, Cambridge CB2 1EW, UK.

[2] Thomas Young Centre and Department of Materials, Imperial College London, London SW7 2AZ, UK.

[3] CIRIMAT, UMR CNRS 5085, Université Paul Sabatier Toulouse III, Toulouse 31062, France.

[4] Department of Chemical and Biomolecular Engineering and Department of Chemistry, University of California, Berkeley, California 94720, United States

[5] RS2E, Réseau Français sur le Stockage Electrochimique de l'Energie, FR CNRS, 3459, Amiens Cedex 80039, France.

[*]Corresponding author's email: acf50@cam.ac.uk

Abstract

Conductive layered metal-organic frameworks (MOFs) have demonstrated promising electrochemical performances as supercapacitor electrode materials. The well-defined chemical structures of these crystalline porous electrodes facilitate structure-performance studies, however there is a fundamental lack in the molecular-level understanding of charge storage mechanisms in conductive layered MOFs. To address this, we employ solid-state nuclear magnetic resonance (NMR) spectroscopy to study ion adsorption in nickel 2,3,6,7,10,11-hexaiminotriphenylene, $Ni_3(HITP)_2$. In this system, we find that separate resonances can be observed for the MOF's in-pore and ex-pore ions. The chemical shift of in-pore electrolyte is found to be dominated by specific chemical interactions with the MOF functional groups, with this result supported by quantum-mechanics/molecular-mechanics (QM/MM) and density functional theory (DFT) calculations. Quantification of the electrolyte environments by NMR was also found to provide a proxy for electrochemical performance, which could facilitate the rapid screening of synthesised MOF samples. Finally, the charge storage mechanism was explored using a combination of *ex-situ* NMR and *operando* electrochemical quartz-crystal microbalance (EQCM) experiments. These measurements revealed that cations are the dominant contributor to charge storage in $Ni_3(HITP)_2$, with anions contributing only a minor contribution to the charge storage. Overall, this work establishes the methods for studying MOF-electrolyte interactions via NMR spectroscopy. Understanding how these interactions influence the charging storage mechanism will aid the design of MOF-electrolyte combinations to optimise the performance of supercapacitors, as well as other electrochemical devices including electrocatalysts and sensors.

1. Introduction

Conductive layered metal-organic frameworks (MOFs) are a class of crystalline materials, that feature high intrinsic porosities and conductivities.[1] These properties have led to promising applications across a diverse range of research fields including energy storage, electrochemical sensing, electrocatalysis, thermoelectrics and spintronics.[2–9] In particular, conductive MOFs of high porosity make ideal electrodes for energy storage in supercapacitors.[3,8,10] The tuneable structure of these materials, achieved through varying the identity of the constituent metal ions and organic linkers, presents an exciting opportunity for understanding molecular-level electrolyte-electrode interactions, and how these interactions impact electrochemical performance. This understanding will be essential for systematic optimisation of electrochemical systems and to overcome the various challenges facing MOF-based supercapacitors, such as their limited charging rates compared to conventional activated carbon-based supercapacitors.[10]

Initial theoretical and experimental studies have begun to investigate the electrochemical interface of conductive layered metal-organic frameworks and to study charge storage in conductive MOFs. Bi *et al.*, used molecular dynamics (MD) simulations to study the charge storage mechanism in MOFs with various pore sizes, including $Ni_3(HITP)_2$, with an ionic liquid electrolyte.[11] This study offered the first insights into the ion distribution at the electrochemical interface for MOFs, revealing distinct distributions of in-pore cations and anions. Further computational studies have built on these foundations by using a hybrid quantum-mechanics/molecular-mechanics (QM/MM) approach to study the interface of the related layered MOF, copper 2,3,6,7,10,11-hexahydroxytriphenylene, $Cu_3(HHTP)_2$, with the benchmark organic electrolyte tetraethylammonium tetrafluoroborate in acetonitrile (NEt_4BF_4/ACN). This latter approach more accurately revealed the charge density distribution at the electric double-layer interface, and was used to assess the favourability of different charging mechanisms for the system.[12] The study suggested that predicted capacitance values for cation-dominated charging mechanisms matched most closely with experimental measurements for this system, and that the preferred anion sorption sites were dependent on the electrode polarity.

Electrochemical quartz crystal microbalance (EQCM) experiments were used to experimentally study the same MOF-electrolyte system employed in the QM/MM study above, $Cu_3(HHTP)_2$ with 1 M NEt_4BF_4/ACN, and supported the cation dominated nature of the charging mechanism.[13] More widely, He *et al.* performed *in-situ* small-angle neutron scattering (SANS) experiments, on $Ni_3(HITP)_2$ cells with an organic electrolyte of sodium triflate in dimethylformamide (DMF).[14] The charging mechanism was found to be dependent on the electrode polarisation and the MOF was proposed to be ionophobic with respect to this electrolyte, with the pores devoid of electrolyte ions in the absence of an applied potential, a scenario which has been predicted to lead to improved performance in nanoporous carbon supercapacitors.[15–17] However, both SANS and EQCM rely on data fitting to separate electrolyte cation, anion and solvent contributions, meaning it is challenging to quantify the charging mechanisms with these techniques. There is an urgent need for new model-free techniques which can directly study the independent interactions of cations and anions at the MOF interface and how this connects with the charging mechanism and performance.

Here we propose the use of solid-state nuclear magnetic resonance (NMR) spectroscopy to reveal ion electrosorption in a layered MOF. NMR has been demonstrated to be a powerful technique to probe and quantify the electrolyte environments in porous carbon electrodes.[18,19] In these materials, 'in-pore' and 'ex-pore' electrolyte environments can be identified from NMR spectra, where the chemical shift dependence of the in-pore resonances are dominated by ring current effects.[20] This leads to a characteristic nucleus independent chemical shift (NICS) of the in-pore environment which is shielded significantly relative to the neat electrolyte.[21] Utilising this assignment, charging mechanisms of porous carbon supercapacitors have been studied by measuring how the in-pore ion populations change upon charging through both *ex-situ* and *in-situ* NMR experiments.[18,22–25] In contrast to EQCM and SANS, NMR can selectively and quantitatively probe cations, anions and solvent species in the system by observing different nuclei and therefore has the potential to resolve some of the existing ambiguity in the literature on MOF electrodes. Indeed, NMR has already been used to identify and quantify 'in-pore' molecular environments in non-conductive MOFs, where the in-pore chemical shift has been found to arise from a competing combination of coordination, solvation and ring-current effects.[26,27] NMR relaxometry has similarly demonstrated the potential to identify guest species in paramagnetic MOFs, as well as probing material porosities, providing several potential useful applications for NMR to be explored on porous conductive MOFs for electrochemical applications.[28–30] Despite this, the application of NMR to study adsorption behaviour of conductive layered MOFs remains unreported.

This study employs NMR for the first time to study the nature of the interaction between organic electrolytes and a conductive layered MOF, and how these interactions impact the charging mechanism. Solid-state NMR reveals separate in-pore and ex-pore electrolyte environments in $Ni_3(HITP)_2$, enabling the study of the electrochemical double layer separately from bulk electrolyte. Our experimental spectra alongside the QM/MM and density functional theory (DFT) calculations reveal that specific interactions between the MOF and the electrolyte dominate the observed chemical shifts and we further find a correlation between measured in-pore ion populations and supercapacitor performance in different MOF batches. Finally, *ex-situ* NMR and *operando* EQCM experiments reveal the cation-dominated charging mechanism of the conductive MOF supercapacitor device. We suggest that exploring the interplay between MOF-electrolyte interactions, charging mechanisms, and performance could lead to the design of improved supercapacitor systems.

2. Results & Discussion

Synthesis and characterisation. To study conductive layered metal-organic framework supercapacitors with NMR spectroscopy, nickel 2,3,6,7,10,11-hexaiminotriphenylene, $Ni_3(HITP)_2$, was selected as it had already been reported to have good supercapacitor performance, and had been used in both experimental and computational studies of supercapacitor charging mechanisms (**Figure 1**).[5,11,14] In this MOF, the Ni^{2+} sites are spd2 hybridised in a square planar configuration, with the resulting low-spin, diamagnetic electronic configuration on the metal site avoiding potential paramagnetic NMR effects caused by the metal centre.[31,32] The syntheses in this work were based on that previously reported by Sheberla *et al.*, and in each case successful synthesis of crystalline $Ni_3(HITP)_2$ was confirmed by powder X-Ray Diffraction (PXRD), with inspection of the diffraction angle of the peaks indicating a consistent crystallographic pore size for all samples (**SI Figure S1**).[33]

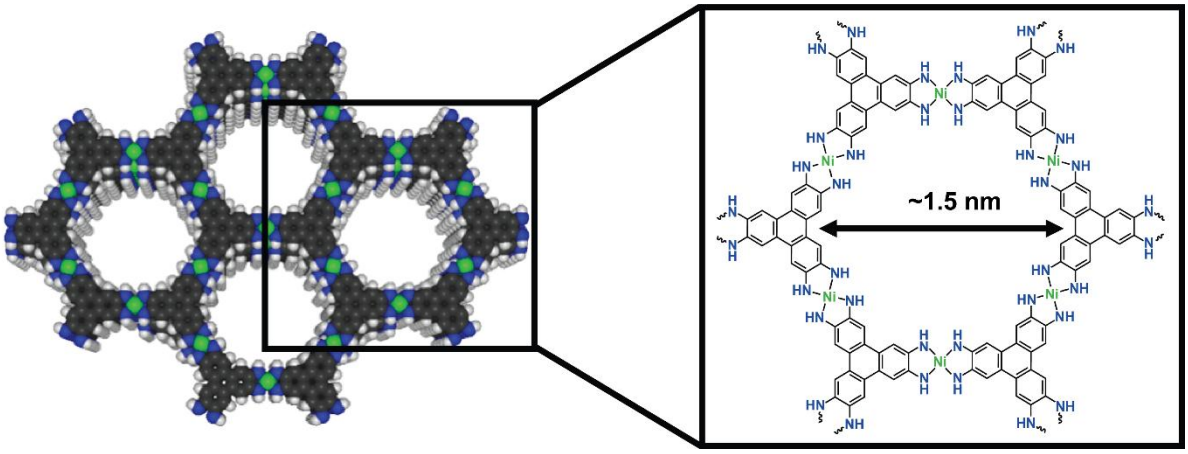

Figure 1: Structure of $Ni_3(HITP)_2$ with enlarged Lewis structure of the hexagonal pore structure.

The samples were subsequently characterised by 77 K N_2 sorption isotherms (**SI Figure S2**), and despite a consistent synthetic procedure, a range of Brunauer–Emmett–Teller (BET) specific surface areas (SSAs) were calculated for the six samples labelled A-F, ranging from 309-894 $m^2\ g^{-1}$ (**SI Figure S2, SI Table S2**). These values are consistent with the range previously reported for this MOF in the literature (260-885 $m^2\ g^{-1}$).[5,32,34–42] We note that even our best samples (samples A and F at 852 and 894 $m^2\ g^{-1}$) have significantly lower BET SSAs than the reported theoretical value of 1370 $m^2\ g^{-1}$ for this MOF, indicating a significant potential for pore blockages from impurities or sample defects.[43] Scanning electron microscopy (SEM) of selected samples confirmed the expected rod-like morphology of the particles (**SI Figure S3**).[5,32,34,35,38–41] Microanalysis highlighted some deviation from the expected stoichiometric quantities of elements, indicating varying levels of defects and impurities in the samples with the additional presence of some chlorine impurities from the starting materials, as previously reported by Sun *et al.* (**SI Table S3**).[38] After characterising the synthesised $Ni_3(HITP)_2$ samples for their crystallinity, porosity, microstructure and chemical composition, the samples were employed in subsequent NMR studies. Unless otherwise specified, results reported below are from samples with a measured BET SSA within 5 % of the highest reported BET SSA in the literature and thus considered to be the highest quality samples.

Investigation of anionic environments with NMR.

To study the electrolyte ion adsorption in $Ni_3(HITP)_2$ using NMR techniques, powdered MOF samples were combined with different loading volumes of 1 M tetraethylammonium tetrafluoroborate in deuterated acetonitrile (1 M NEt_4BF_4/d_3ACN) electrolyte, and ^{19}F NMR spectra were recorded to investigate the BF_4^- anion environments. (**Figure 2a**). Each ^{19}F NMR spectrum revealed two resonances, indicative of two major BF_4^- anion environments in the system, which can be initially assigned to 'in-pore' and 'ex-pore' environments (**SI Figure S4a**). The peak at approx. −145.5 ppm is assigned to in-pore anions as it is shifted by a greater extent away from the neat electrolyte due to MOF-anion interactions, while the peak at approx. –148.5 ppm is much closer to the neat electrolyte's chemical shift and is assigned to ex-pore BF_4^- species. The in-pore peak is additionally identified by more intense magic-angle spinning (MAS) sidebands, which from fitting various spectra of various

samples with a chemical shift anisotropy (CSA) model (**SI Table S4**) consistently indicated a greater anisotropy experienced in this confined electrolyte environment compared to the more mobile ex-pore electrolyte despite variation in the absolute CSA value between samples.

Our peak assignments were further supported by integration of the NMR spectra at variable loadings (**SI Figure S5a**). At the lowest loading, the in-pore environment dominates, but upon increasing the solvent loading this peak grows slowly compared to the proposed ex-pore environment, which dominates at higher electrolyte loadings where the in-pore environment i.e. the electrolyte-accessible porosity of the MOF, becomes saturated. A series of analogous adsorption experiments on $Ni_3(HITP)_2$ composite electrode film gave rise to the same two environments, following the same trend on variation of electrolyte loading (**SI Figure S6**).

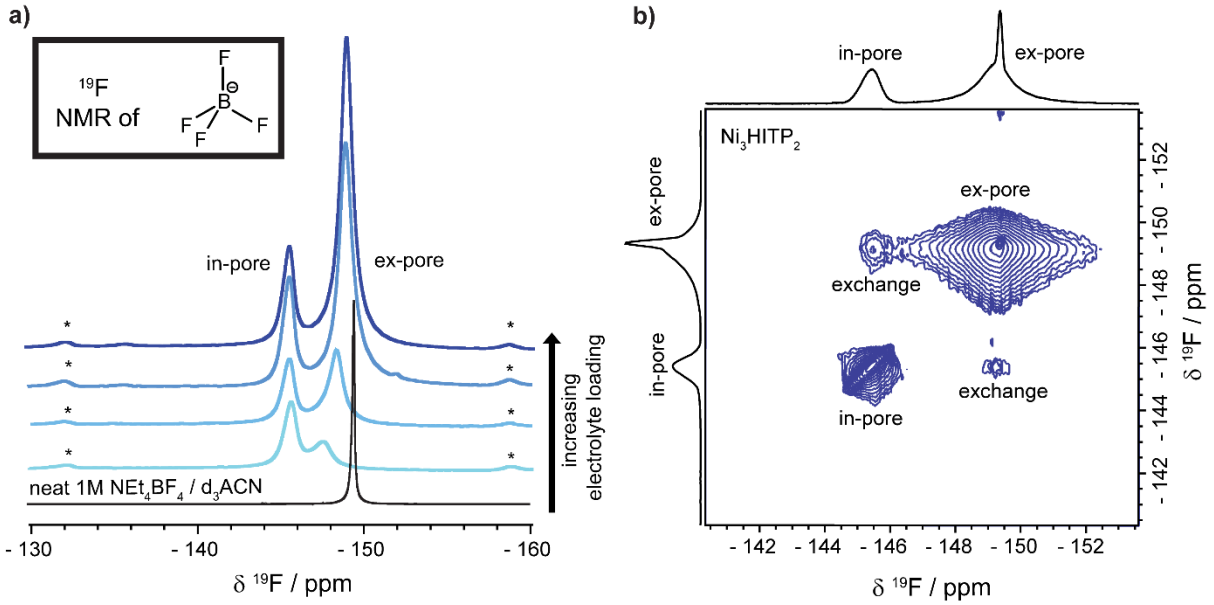

Figure 2: ^{19}F solid-state NMR (9.4 T) experiments at 5 kHz MAS **a)** Quantitative spectra of powder $Ni_3(HITP)_2$ sample A at various loadings of 1 M NEt_4BF_4/d_3ACN electrolyte compared to ^{19}F NMR of the neat electrolyte. Spinning sidebands for the in-pore peak are denoted by *. The darkening shade of blue indicates progressively higher electrolyte loadings, from light blue to dark blue: 0.3, 0.5, 1.2, 1.3 g of electrolyte per g of $Ni_3(HITP)_2$ **b)** EXSY experiment with a mixing time of 50 ms showing chemical exchange between in-pore and ex-pore anions in a composite film of $Ni_3(HITP)_2$ sample A soaked with 1 M NEt_4BF_4/d_3ACN electrolyte.

Having, made these initial assignments, the ion dynamics of the system were investigated. Interestingly, the peak assigned as 'ex-pore' shifts towards the neat electrolyte peak at increasing electrolyte loading (**Figure 2a**, **SI Figure S5b**). This change in chemical shift could not be accounted for purely by those expected for variation in the local electrolyte concentration (**SI Figure S7**), which suggests this peak is impacted by fast exchange on the NMR timescale between truly unconfined electrolyte in the 'ex-pore' environment, and a smaller proportion of electrolyte which is influenced by the MOF, likely close to the pore openings such that it is easily accessible for exchange. Exchange spectroscopy (EXSY) was used to further reveal the slow exchange between in-pore and ex-pore environments, which manifests as cross peaks appearing on a timescale of tens of milliseconds (**Figure 2b**). Despite these various exchange contributions, the adsorption experiments on $Ni_3(HITP)_2$ confirmed the presence of two key environments, in-pore and ex-pore, analogous to those seen in adsorption NMR studies on activated porous carbons.[19]

Interestingly, the 'in-pore' BF_4^- peak for $Ni_3(HITP)_2$ is positively shifted from the neat electrolyte resonance, quantified by $\Delta\delta = \delta_{\text{in-pore}} - \delta_{\text{neat}} = +3.9$ ppm (**Figure 3a**). This contrasts with the negative $\Delta\delta$ values seen in NMR studies of ion adsorption in porous carbons, where ring current shielding effects dominate the $\Delta\delta$ values, leading to a nucleus independent chemical shift.[19] As a result, in porous carbons, the observed $\Delta\delta$ remains constant when varying the NMR active nucleus studied, or the electrolyte components. In MOFs, other non-covalent binding interactions may dominate the chemical shifts, with one possibility in $Ni_3(HITP)_2$ being hydrogen-bond interactions between the BF_4^- anions and the N-H moiety of the HITP linker.[20,26]

To investigate the origin of the observed Δδ values in $Ni_3(HITP)_2$, both the studied NMR active nucleus and the electrolyte anion were independently varied (**Figure 3**, **SI Table S5**). Studying the same sample in the original electrolyte of 1 M NEt_4BF_4/d_3ACN with ^{11}B NMR as a second probe of BF_4^-, the two peaks are no longer well-resolved (**Figure 3b**). On deconvolution Δδ for the ^{11}B spectrum was found to be just +0.7 ppm (**SI Table S5**). The significant difference in the ^{19}F and ^{11}B Δδ values for $Ni_3(HITP)_2$ is in contrast to previous findings on porous carbons.[19] Indeed, previous work on a microporous carbide-derived-carbon showed very similar ^{19}F and ^{11}B Δδ values of +5.5 ppm and +5.7 ppm respectively.[19] These shifts are dominated by a ring-current shift, which is assumed to be similar on average for both nuclei due to the rapid rotation of the BF_4^- anion in the electrolyte.[20] Therefore, the observed nucleus-*dependent* effects in $Ni_3(HITP)_2$ suggest a different dominant chemical shift mechanism compared to porous carbons.

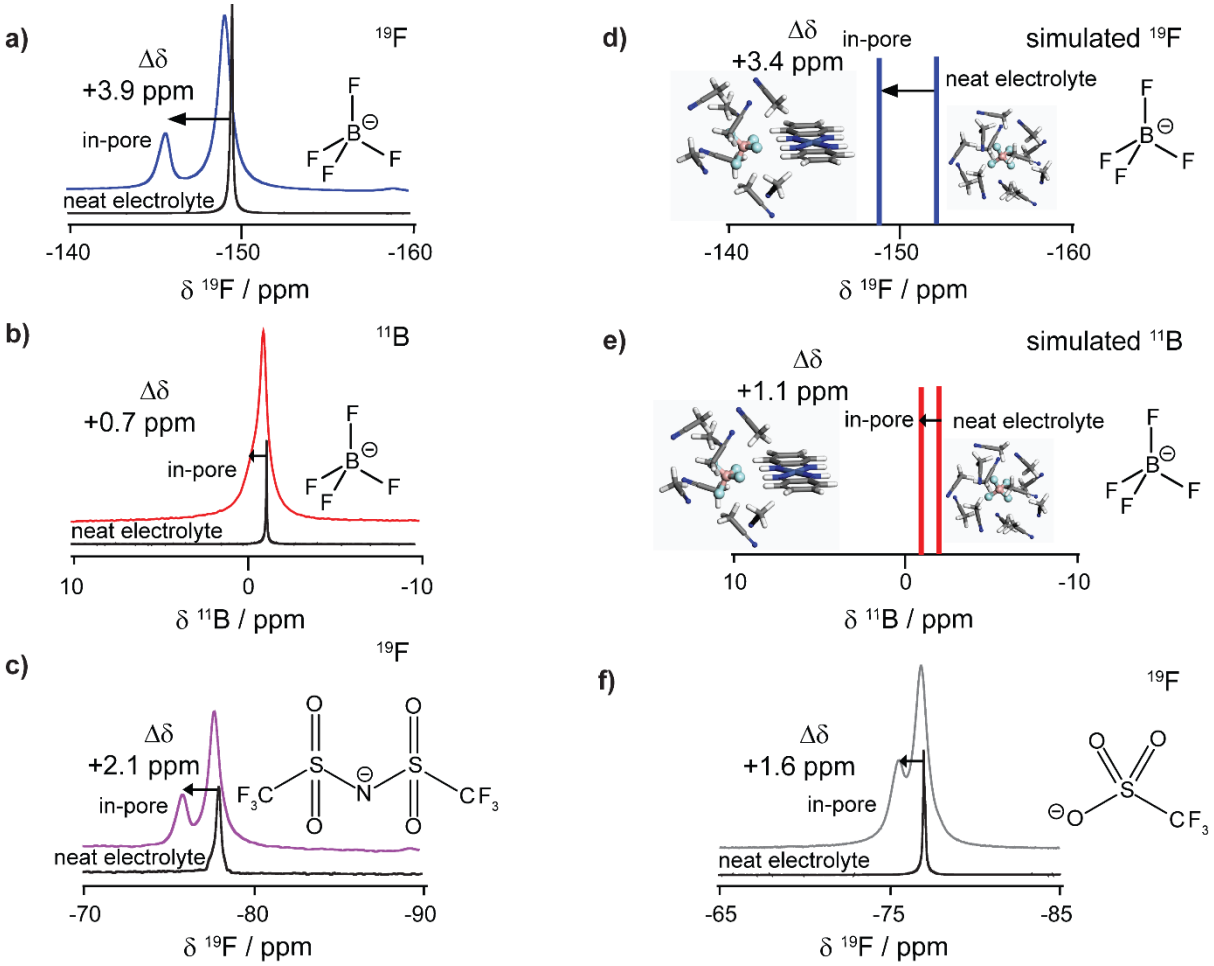

Figure 3: a) ^{19}F and **b)** ^{11}B solid-state NMR (9.4 T) spectra of $Ni_3(HITP)_2$ soaked with 1 M NEt_4BF_4/d_3ACN compared to neat electrolyte **c)** ^{19}F solid-state NMR (9.4 T) spectra of $Ni_3(HITP)_2$ soaked with 1 M NEt_4TFSI/d_3ACN compared to neat electrolyte **d)** ^{19}F and **e)** ^{11}B simulated NMR spectra of tetrafluoroborate anion close to $Ni_3(HITP)_2$ MOF fragment compared to in bulk acetonitrile. Spectra are schematic to show the simulated chemical shift, the line width is not indicative of the peak width. **f)** ^{19}F solid-state NMR (9.4 T) spectra of $Ni_3(HITP)_2$ soaked with 1 M $NaSO_3CF_3$/DMF compared to neat electrolyte. All experimental spectra used $Ni_3(HITP)_2$ Sample A and are recorded in the quantitative regime with an MAS rate of 5 kHz.

To continue exploring the origin of the Δδ values in $Ni_3(HITP)_2$, the ion investigated via NMR was varied. Preliminary data showed poor resolution in ^1H NMR spectra, suggesting a small Δδ and making identification and accurate quantification of NEt_4^+ cation environments difficult (**SI Figure S8**). Further, ^{19}F NMR was used to investigate the adsorption environments for $TFSI^-$ anions in $Ni_3(HITP)_2$ in 1 M tetraethylammonium bis(trifluoromethylsulfonyl)imide (NEt_4TFSI) in acetonitrile electrolyte. The same two anion environments were evident in the spectrum, but with a measured Δδ for the 'in-pore' environment of +2.1 ppm (**Figure 3c, SI Table S5**). Hence, these nucleus and anion-*dependent* results therefore demonstrate ring-current effects, whilst perhaps a contributor, are not dominant for this system, leading to a hypothesis that non-covalent interactions dominate the observed shifts. We further

propose that the Δδ value is related to the strength of the interaction between the anions and the MOF functionality. DFT calculations confirmed a larger charge density on the fluorine atoms for the BF_4^- anion compared to the $TFSI^-$ anion as expected, leading to a stronger specific interaction alongside a larger observed Δδ. Additionally,^{11}B NMR above gave rise to a low Δδ of just +0.7 ppm as boron, unlike fluorine, is not directly participating in a specific interaction with the MOF pore wall. These experimental therefore results support the hypothesis that the MOF-electrolyte interaction strength is modulated by the charge density on the fluorine (**SI Figure S9**).

To further investigate the proposed specific MOF-electrolyte interactions, chemical shift calculations were carried out on structural fragments extracted from hybrid QM/MM simulations of the $Ni_3(HITP)_2$ - NEt_4BF_4/ACN system (see SI and **SI Figure S10** for details). The simulations predicted respective ^{19}F and ^{11}B NMR Δδ values of +3.4 ppm and +1.1 ppm calculated for a BF_4^- anion in close proximity to a MOF fragment, compared to an anion in bulk acetonitrile (**Figure 3d, e, SI Table S5**), in close agreement with the experimental values. Furthermore, simulations in the absence of an applied electrochemical potential, show that the anions are distributed over a range of sites within the pore, but overall favour sites close to the MOF pore walls, adjacent to the N-H groups (**SI Figure S11**). Collectively, these results support the hypothesis that the ^{19}F and ^{11}B chemical shifts arise predominantly from a hydrogen-bond type interaction of the fluorine atoms with the hydrogens in the MOF N-H groups and that the value of Δδ may be linked to the strength of that interaction. It is these specific interactions which are responsible for the high resolution of the in-pore environment in the ^{19}F NMR. Thus, anions closer to the centre of the MOF pore would have a lower Δδ if measured directly, but as they are in fast exchange with the anions on the edge of the pores, the observed Δδ is a weighted average of all the anion environments. This specific anion-MOF specific interaction may also explain why the same effect is not seen in the ^{1}H NMR spectra of the electrolyte cations, which will not undergo the same favourable hydrogen-bonding interaction with the MOF (**SI Figure S8**).

With the opportunity to study this MOF-electrolyte anion interaction, we further employed NMR to study a system previously reported to have negligible ion uptake (at null potential), by soaking $Ni_3(HITP)_2$ with 1 M sodium triflate in dimethyl formamide ($NaSO_3CF_3$/DMF) electrolyte (**Figure 3f**).[14] The resulting spectrum closely resembles those of the other organic electrolyte systems, with two peaks which we assign to in-pore and ex-pore environments, and a ^{19}F Δδ of +1.6 ppm. The charge density on the fluorine atoms in the $SO_3CF_3^-$ anion from DFT calculations is similar to the $TFSI^-$ anion, supporting a similarly weak interaction with the MOF compared to BF_4^- (**Figure 3a**) and thus a smaller Δδ (**SI Figure S9**). The larger Δδ relative to $TFSI^-$ (**Figure 3c**) is likely a result of the smaller anion size of $SO_3CF_3^-$ allowing on average a closer approach of the anion to the MOF than $TFSI^-$. As before, note that significant spinning sidebands are present only for the more anisotropic in-pore environment in this system, supporting our assignments (**SI Figure S12, SI Table S4**). Overall, our results suggest that there is in fact a significant in-pore anion population even without charging, in contrast with the negligible ion uptake previously reported by He *et al*. These findings highlight the significant power of ^{19}F NMR to probe ion adsorption and specific MOF-electrolyte interactions.

Correlating In-pore Anion Population in the Absence of Applied Potential to Electrochemical Performance. ^{19}F NMR adsorption experiments, analogous to those previously described, were subsequently evaluated as a tool to predict the electrochemical performance of $Ni_3(HITP)_2$ samples. Two samples with contrasting BET SSAs, sample A at 852 $m^2\,g^{-1}$, and sample B at 309 $m^2\,g^{-1}$, were selected and made into composite electrode films for further BET measurements (**Figure 4a**), NMR adsorption experiments (**Figure 4b**), and electrochemical performance tests (**Figure 4c**, **SI Table S2**). Adsorption experiments were performed at high electrolyte loadings to saturate the porosity of the MOF and probe the electrolyte-accessible in-pore volume (**SI Table S2**). Sample A was found to have a higher in-pore anion population (defined by mmol of in-pore anions per gram of MOF), evident from the larger integral of the in-pore peak in adsorption experiments (**Figure 4b**). Furthermore, we note a difference in the peak shape of the ex-pore environments between the two samples which we attribute to differences in ion exchange rates.

Importantly, Sample A demonstrated a higher gravimetric capacitance measured from galvanostatic-charge-discharge (GCD) experiments (**SI Table S2**), which was also supported by a larger cyclic voltammogram (CV) area for a symmetric supercapacitor cell (**Figure 4c**). The CVs for both samples over a cell voltage window of 1.0 V qualitatively resemble the electric double-layer behaviour previously reported for this system.[5,41] However, with a gravimetric capacitance of 160 F g^{-1} at a current density of 0.05 A g^{-1} (0.3 mA cm^{-2}), Sample A exceeds the electrochemical performance reported in the literature for the same system (up to 111 F g^{-1} at a current density of 0.05 A g^{-1}), and competes closely with the

gravimetric capacitance of $Ni_3(HITP)_2$ with aqueous sodium sulfate electrolyte (170 F g^{-1} at a current density of 0.1 mA cm^{-2}) reported by Nguyen *et al.*[5,41,44] With a gravimetric capacitance of 62 F g^{-1}, Sample B falls within the range reported by Borysiewicz *et al.*.[41] The batch-to-batch variation observed in electrochemical performance may be linked to variations in MOF morphology, as has previously been reported for $Ni_3(HITP)_2$.[41] Morphology differences would also be expected to give rise to changes in exchange rate between the in-pore and ex-pore environments, which would explain the significant difference in peak-shape of the ex-pore environment.

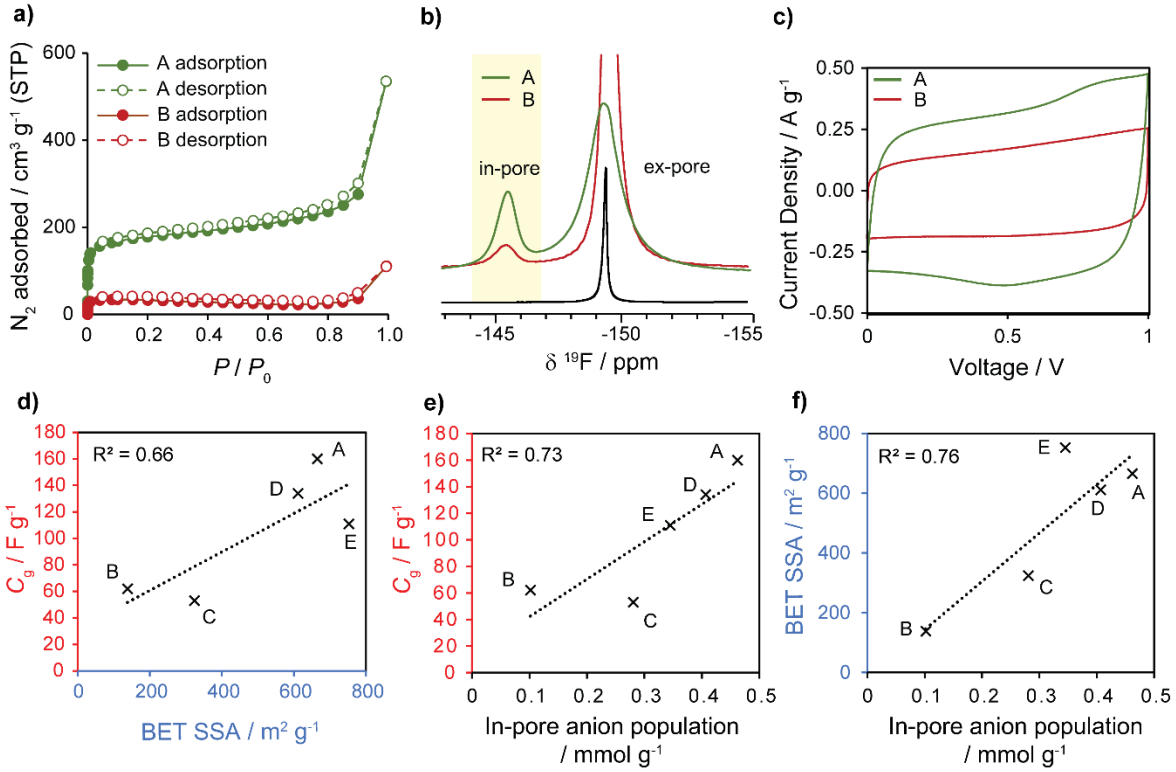

Figure 4: a) N_2 gas sorption isotherms at 77 K of $Ni_3(HITP)_2$ composite films of sample A (high BET SSA) and B (low BET SSA) **b)** Quantitative ^{19}F solid-state NMR (9.4 T) spectra at 5 kHz MAS of $Ni_3(HITP)_2$ composite films of sample A and B at saturated electrolyte loading volumes of 1 M NEt_4BF_4/d_3ACN, compared to neat electrolyte spectrum; differences in intensity of the in-pore peak are highlighted **c)** CVs at 5 mV s^{-1} of symmetric supercapacitors with $Ni_3(HITP)_2$ samples A and B as the active electrode material. The small faradaic contribution prominent in the CV for Sample A is attributed to the previously reported quasi-reversible oxidation process of the MOF, reported to be likely centred on the linker molecule.[5] Correlations between **d)** BET SSA and gravimetric capacitance, **e)** In-pore anion population and gravimetric capacitance, and **f)** In-pore anion population and BET SSA for the five $Ni_3(HITP)_2$ composite film samples studied. All samples reflect a single gas sorption measurement except sample E which is represented as an average of two measurements. Gravimetric capacitances at a current /density 0.05 A g^{-1} were measured from galvanostatic-charge-discharge (GCD) experiments.

To assess in more detail how well NMR adsorption experiments in the absence of an applied potential predict electrochemical performance, gravimetric capacitance (**SI Table S2**) was plotted as a function of both the BET SSA (**Figure 4d, SI Figure S13**) and in-pore anion population obtained by NMR for composite films of five samples of $Ni_3(HITP)_2$ samples (A-E; **Figures 4e, SI Figure S14**). We observe that the NMR characterisation provides a rough indication of gravimetric capacitance through the correlation of the two properties ($R^2 = 0.73$) (**Figure 4e**). For our samples, we found adsorption NMR to predict gravimetric capacitance to a similar accuracy as BET SSA ($R^2 = 0.66$), which is conventionally used to screen conductive MOF quality (**Figure 4d**). As such, there is also a some correlation between in-pore ion population and BET SSA itself ($R^2 = 0.76$), highlighting the ability of NMR to effectively probe porosity of layered MOFs (**Figure 4f**). However, since our NMR experiments probe electrolyte-accessible pore volume, whereas the BET analysis is derived from N_2 gas sorption data, we anticipate some deviation between the correlations. This is highlighted by the unexpectedly high BET SSA for Sample E, given its associated gravimetric capacitance and in-pore anion adsorption. Nevertheless, we see that the adsorption NMR experiments still accurately reflect the gravimetric energy storage

performance in this sample. Due to the anomalously high BET SSA of the composite film of sample E, the in-pore anion population was also plotted with the BET SSA of the powder MOF samples to further probe the relationship between NMR adsorption and gas sorption experiments (**SI Figure S15**). This showed an improved correlation (R^2 = 0.99), supporting our initial results. Importantly, as our ^{19}F NMR experiments take only minutes to acquire compared to hours/days for gas sorption measurements, this work shows that adsorption NMR experiments could be used as an alternative to gas sorption where higher throughput screening of MOF samples is required (**Figure 4e, 4f**).

***Ex-situ* NMR Charging Experiments.**

To explore the capacitive charging mechanism of $Ni_3(HITP)_2$, this MOF was employed as an active electrode material in *ex-situ* supercapacitor experiments, for which NMR is performed after charging and disassembly of the supercapacitor (**Figure 5**). *In-situ* NMR measurements, performed in real-time on a charging supercapacitor, were not possible due to lack of spectral resolution in the absence of magic-angle spinning (**SI Figure S16a**). *Ex-situ* ^{19}F NMR spectra for all the electrodes showed the two expected resonances, corresponding to in-pore and ex-pore BF_4^- anion environments (**Figure 5a, SI Figure 4b, c**). Interestingly, a systematic shift of the in-pore resonance was also observed as the charging voltage was varied (**Figure 5b**). The experiments were conducted with 1 M NEt_4BF_4 in propylene carbonate (PC), a less volatile solvent, in addition to the original 1M NEt_4BF_4 in acetonitrile electrolyte (**SI Figure S16b**). Similar results were obtained for the two electrolyte systems, despite concerns about solvent evaporation with the acetonitrile-based electrolyte (**SI Figure S16c**).

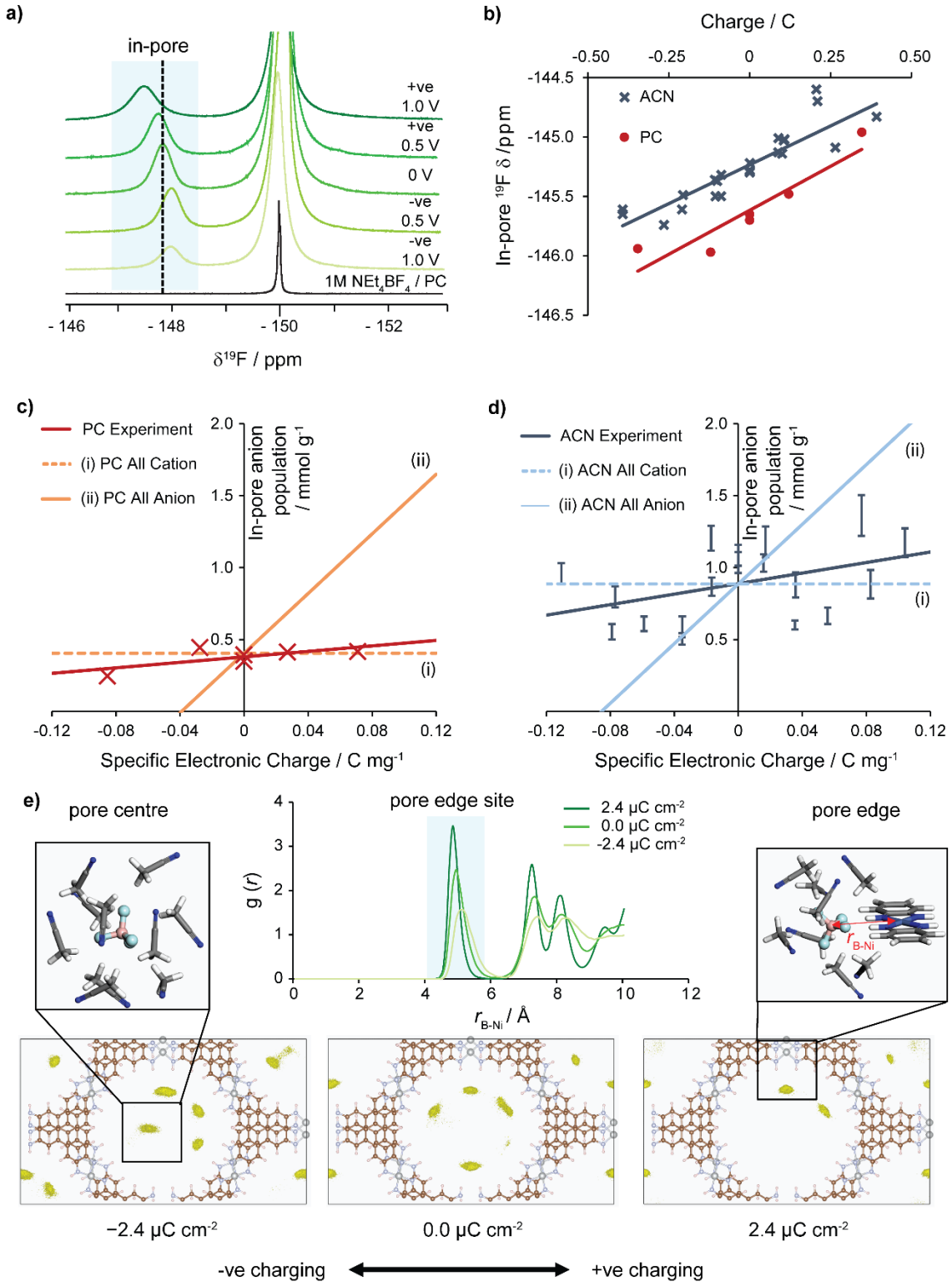

Figure 5: Studies on charging $Ni_3(HITP)_2$ supercapacitor electrodes with organic electrolytes. In the *ex-situ* experiments, symmetric supercapacitors with were held at a constant voltage for one hour as the current was monitored, and then disassembled, with NMR performed separately on each of the electrodes after disassembly. **a)** ^{19}F solid-state NMR (9.4 T) spectra at 25 kHz MAS of *ex-situ* electrodes of $Ni_3(HITP)_2$ with 1 M NEt_4BF_4 in propylene carbonate (PC) compared to neat electrolyte; to obtain peak resolution for accurate fitting, a higher MAS rate of 25 kHz was required for samples with propylene carbonate solvents (**SI Figure S16d**). **b)** Correlation between in-pore chemical shift and electrode charge for 1M NEt_4BF_4 in deuterated acetonitrile (ACN), and propylene carbonate (PC). Measured in-pore ion population against specific electronic charge compared to theoretical scenarios in which all electrode charge storage is accounted for by exclusively (i) cation, or (ii) anion movement, with intercept fixed at the same value as the regression line for ease of comparison of their gradients,

for an electrolyte of 1 M NEt_4BF_4 in **c)** propylene carbonate (PC) and **d)** deuterated acetonitrile (ACN) **e)** Top middle: Radial distribution function, $g(r)$ as a function of distance between the boron atom of BF_4^- and nickel in $Ni_3(HITP)_2$, the peak in the highlighted region corresponds to the pore-edge environment. Bottom row: QM/MM of simulated anion populations, highlighted in yellow, for 1 M NEt_4BF_4 electrolyte in $Ni_3(HITP)_2$, under negative charging (left), zero charge (middle), and positive charging (right). The isosurface level is 0.003 e $bohr^{-3}$. Simulations follow the cation-dominated charging mechanism observed experimentally. Simulated anion population symmetry is not fully maintained in 5 ns sampling time due to its strong binding affinity to the electrode. Two key anion sites are identified as pore centre (top left) and pore edge (top right).

Through using calibration experiments, quantitative in-pore BF_4^- populations were obtained at different charging voltages (**SI Figure S17**). For both the propylene carbonate (**Figure 5c**), and the acetonitrile electrolytes (**Figure 5d**), the in-pore anion population was plotted against the specific electronic charge of the electrode, alongside different theoretical scenarios. First, (i) an 'all cation' scenario in which the cations account for all of the electrode's charge storage, and there is no net change in the in-pore anion population, *i.e.* charge is stored through cation adsorption (counter ion adsorption) for the negative electrode, and through cation desorption (co-ion desorption) for the positive electrode. And in the second case (ii) an 'all anion' scenario in which the anions account for all the electrode's charge storage. Both cases are for illustration of the gradient only, and the intercept is fixed to match that of the experimental regression slope. By comparison of the experimental slope from regression with the theoretical scenarios, the anions accounted for 9±13 % of the total charge storage in a propylene carbonate electrolyte, and 18±20 % in an acetonitrile electrolyte (95% confidence interval, see SI for details). Therefore, the experimental result for both electrolytes is closer to the "all cation" scenario. This gives confidence that regardless of the organic solvent, cations are the major contributor to charge storage in $Ni_3(HITP)_2$. This finding supports the cation-dominated charging mechanism proposed from theoretical and experimental work for the related MOF $Cu_3(HHTP)_2$.[12,13] Therefore, whilst in-pore anion population was earlier shown to serve as a useful indicator of electrolyte-accessible pore volume and hence electrochemical performance (**Figure 4e**), the anions themselves are not primarily responsible for the charge storage in these systems.

Despite a relatively small change in the total in-pore anion population on charging, it was possible to detect more subtle charging processes by monitoring the chemical shift of the in-pore environment. It was found that the in-pore chemical shift in both electrolytes was strongly correlated with the charge stored in the electrode, giving rise to a linear relationship (**Figure 5b**). We propose that this variation of the $\Delta\delta$ value is related to changes in both the distribution of anions between pore-centre and pore-edge sites (which are expected to be in fast exchange on the NMR timescale) and the strength of the specific interaction between the anion and the MOF N-H sites. Further QM/MM simulations with charging were used to investigate this behaviour (**Figure 5e, SI Table S3**). On negative charging (**Figure 5e,** bottom left), a dramatic change in anion distribution is observed relative to the uncharged scenario (**Figure 5e,** bottom middle), with a significant shift in anions towards the pore centre. This can be attributed to the now less favourable interactions with the net negative MOF pore edge. The drop in anion population at the pore edge site is indicated by the reduced integral of the peak around 5 Å in the radial distribution function (**Figure 5e,** top middle). Any anions remaining close to the pore edge will also experience a weaker H-bonding interaction owing to a smaller partial positive charge on the H atom of the MOF N-H groups, and this is amplified by a shift of the pore-edge environment away from the MOF walls also seen in the radial distribution function, with the peak around 5 Å shifting to a greater $r_{B\text{-}Ni}$ distance (**Figure 5e,** top middle). These synergistic effects lead to a reduced $\Delta\delta$ value during negative charging. Conversely, on positive charging (**Figure 5e,** bottom right), the anions interact more favourably with the edge of the MOF, where the N-H groups become more positively charged, and so anions migrate towards the pore boundary of the MOF, resulting in a higher pore-edge population in closer proximity to the N-H groups (**Figure 5e,** top middle). Therefore, an increase in the average $\Delta\delta$ value is observed. A similar behaviour of anion rearrangements has previously been proposed in the related MOF, $Cu_3(HHTP)_2$.[12] These experimental observations were found to be in qualitative agreement with calculated ^{19}F chemical shift values with charging of a MOF fragment using implicit solvation of an adsorbed BF_4^- anion (**SI Figure S18**). Therefore, whilst the total in-pore anion population is almost invariant as cations dominate the charge storage for these conductive layered MOF systems, NMR has the power to track subtle changes in the anion distribution within the pore structure and the strength of the MOF-electrolyte interaction.

Operando EQCM experiments.

As ^1H NMR could not accurately quantify the environments of the cations due to poor resolution of the proton spectra (**SI Figure S7**), EQCM experiments were performed with $Ni_3(HITP)_2$ with 1 M NEt_4BF_4

in acetonitrile electrolyte to further investigate the charging mechanism (**Figure 6**). In EQCM, the frequency change, Δ*f*, of a crystal is measured and used to determine the change in mass, Δ*m,* of an electrode during charging via Sauerbrey's equation, as long as the gravimetric approach is valid (see SI for details, **SI Figure S19**).[45] This change in mass can be attributed to movement of cations, anions and solvent into and out of the electrode. To prevent possible decomposition reactions that occur on the MOF/Au electrode of the EQCM cell, the potential window was restricted to +200 mV to +500 mV *vs.* Ag during the EQCM experiment (**Figure 6a**; CVs shown in outside lines with frequency change (Δ*f)* shown inside). Given that the open circuit potential of the electrode, prior to any polarisation, was +284 mV relative to Ag, the selected potential window covers in part both positive and negative charging regimes of the *ex-situ* NMR experiments above. Furthermore, by using a slow voltage sweep of 1 mV s^{-1}, we assume that the mechanistic charging processes observed via EQCM can be directly compared to the results of the earlier *ex-situ* NMR experiments, which used constant voltage holds.

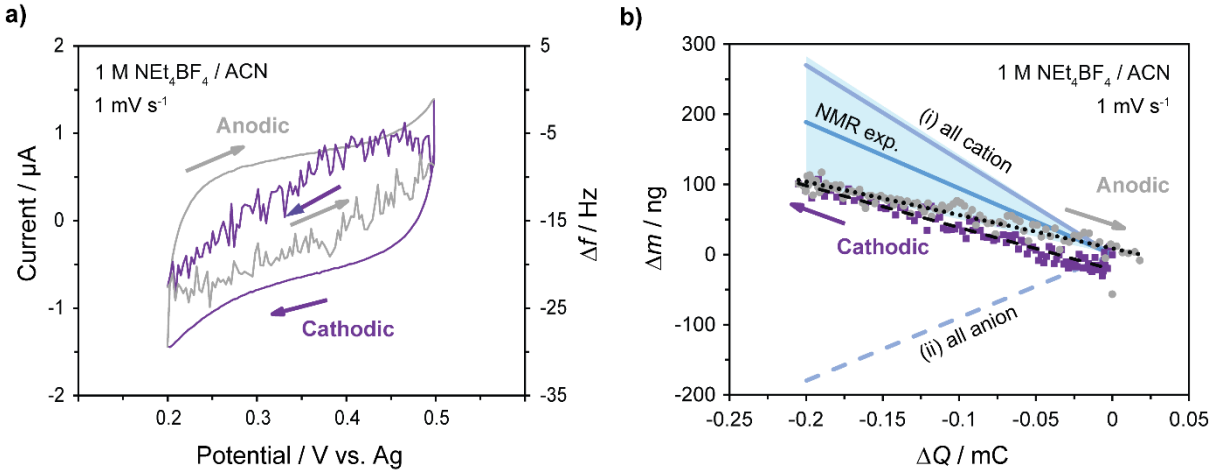

Figure 6: a) CV (outside lines) and EQCM frequency response (inside lines) of $Ni_3(HITP)_2$ with 1 M NEt_4BF_4/ACN electrolyte, at a scan rate of 1 mV s^{-1}. The potential range was restricted to +200 to +500 mV *vs.* Ag to avoid the possible decomposition reactions at the MOF/Gold electrode of the EQCM cell. **b)** Plot of experimental electrode mass change, Δ*m*, calculated according to Sauerbrey's equation from the frequency response, Δ*f*, shown in (a), against accumulated charge (Δ*Q*). Δ*Q* was calculated by integrating the current against time for the CVs and setting the charge at the electrode potential of +500 mV *vs.* Ag to zero. Δ*f* and Δ*m* are considered separately for cathodic (purple) and anodic (grey) polarisations. The average mass change is given by the dashed line (cathodic scan) and the dotted line (anodic scan). These experimental results are compared with theoretical scenarios, in which all electrode charge storage is accounted for by exclusively (i) cation or (ii) anion adsorption, and the predicted range of Δ*m* calculated from *ex-situ* NMR experiments with an 18±20 % anion contribution indicated by the shaded blue region. All these scenarios exclude any contributions from movement of solvent.

A reversible and negative correlation between Δ*m* and Δ*Q* was found during cathodic polarisation (**Figure 6b**), which by comparison with the (i) all cation and (ii) all anion scenarios described above indicates that cations are the dominant charge carriers in this system.[45] Therefore, the mass increase with negative electronic charge accumulation indicates net cation adsorption in the cathodic charging process, while a reversible net cation desorption process is observed in the anodic regime. Importantly, this agrees qualitatively with the *ex-situ* NMR results above and confirms the dominant contribution of the cations to the charging mechanism. The slope of the EQCM data on both cathodic and anodic charging corresponds to a relatively small change in mass on charging relative to the range expected from the experimental *ex-situ* NMR data (**Figure 6b**). This result suggests that, in addition to the dominant cation adsorption during cathodic charging, there must be a net loss of solvent and or/anion desorption, and vice versa on anodic charging. As only the net mass change is recorded in EQCM experiments, it is difficult to accurately quantify the absolute solvent and/or anion movement as molecules may simultaneously be moving into and out of the pores during both charging and discharging. To investigate the solvent contribution to the charging mechanism further, ^{2}D NMR of the deuterated acetonitrile solvent in 1 M NEt_4BF_4/d_3ACN was attempted, with the aim to quantify the 'in-pore' solvent environment (**SI Figure S20**). However, due to poor resolution, fitting these spectra is associated with high uncertainty, and coupled with partial evaporation of acetonitrile in *ex-situ* measurements, makes the application of NMR limited in studying the solvent in this system. Nevertheless, this works highlights the complementary nature of EQCM together with NMR to study anion, cation and solvent contributions to the charging mechanism of layered MOFs in supercapacitor

devices. Qualitatively, a cation-dominated charging mechanism is observed in both NMR and EQCM charging experiments for this MOF system, although measuring the quantitative agreement in the percentage contribution of anion movement to charge storage is not possible.

Interestingly, the cation dominated nature of this charging mechanism is consistent with EQCM studies on the related MOF $Cu_3(HHTP)_2$ with 1 M NEt_4BF_4/ACN electrolyte.[13] The greater contribution of the cations compared to anions in charge storage of these systems suggests that the cation identity may be most closely linked to the overall electrochemical performance. Gittins *et al*. previously demonstrated the impact of increasing the alkyl chain length in this family of cations, but further exploration of electrolytes is needed to improve electrochemical performance beyond that for 1 M NEt_4BF_4/ACN electrolyte. Conversely, this work may suggest that the cations are only the dominant contribution to charge storage in this system due to relatively strong BF_4^- anion-MOF interactions. If the relative strengths of the interactions between the anions and the cations with the MOF could be systematically modified, this could be exploited to control the extents to which each ion contributes to charge storage. Controlling the charging mechanism in this way would likely also give rise to higher capacitive performance.

3. Conclusion

This work has demonstrated the application of solid-state NMR spectroscopy for understanding the ion adsorption and charge storage mechanisms of conductive layered metal-organic frameworks. Importantly, our NMR spectra of $Ni_3(HITP)_2$ soaked with a traditional supercapacitor organic electrolyte reveal distinct resonances for in-pore and ex-pore BF_4^- anions, providing the opportunity to study the electric double layer in these materials during charging. The chemical shift of the in-pore resonance was further revealed to be determined by specific anion-MOF interactions, an observation which was supported by QM/MM and DFT simulations. Solid-state NMR has also demonstrated potential for high throughput screening of the electrochemical performance of layered MOFs, with significantly improved efficiency compared to traditional N_2 gas sorption experiments. Furthermore, for the first time, *ex-situ* NMR measurements were used to gain experimental insights into the charging mechanism of a layered MOF, $Ni_3(HITP)_2$, with organic electrolytes, and revealed only a minimal contribution of anions. Subtle changes in the in-pore chemical shift were seen on charging, which in combination with QM/MM simulations, are linked to a redistribution of anions between two key in-pore environments. Given the coupled experimental challenges of obtaining peak resolution in NMR (i) under static conditions and (ii) of the cation environments in this system, we emphasise the need for both the development of spinning *in-situ* NMR systems and combining NMR with other techniques for a complete mechanistic study.[47,48] As such, EQCM experiments supported the idea that cations are the dominant charge carriers in this system, and additionally highlighted the importance of the solvent in the charging mechanism, a contribution which is yet to be fully understood in these systems. The specific MOF-electrolyte interactions observed by NMR in these systems is in contrast with activated carbons typically used in supercapacitors and therefore presents a unique opportunity for MOF-based systems. These interactions may be explored and exploited further to modify their strength, and therefore to both modulate the charging mechanism, and optimise supercapacitor performance. As such, this work offers a number of pathways for solid-state NMR to be used to aid the future design of supercapacitors.

Data Availability

All raw experimental data files are available in the Cambridge Research Repository, Apollo, with the identifier DOI: https://doi.org/10.17863/CAM.107715

Acknowledgements

C.J.B acknowledges a Walters-Kundert Studentship (Selwyn College, Cambridge). J.W.G thanks the School of Physical Sciences (Cambridge) for the award of an Oppenheimer Studentship. A.C.F acknowledges the ESPRC (EP/X042693/1) for Horizon Europe guarantee funding for an ERC Starting grant, and a UKRI Future Leaders Fellowship (MR/T043024/1). K.G thanks a grant from the China Scholarship Council. S.S acknowledges funding from Leverhulme Trust for funding (RPG-2020-337). P.S. and P.L.T. acknowledge the support from Agence Nationale de la Recherche (Labex Store-ex) and ERC Synergy Grant MoMa-Stor #951513. X. L. acknowledges PhD funding from the Cambridge Trust and the China Scholarship Council. This work was supported by EPSRC project EP/X037754/1. Via our membership of the UK's HEC Materials Chemistry Consortium, which is funded by EPSRC

(EP/X035859/1), this work used the ARCHER2 UK National Supercomputing Service (http://www.archer2.ac.uk).

Supporting Information

Additional experimental and simulation details, methods and materials, detailed discussion of NMR and EQCM analysis, supporting figures including PXRD, SEM, gas sorption isotherms, additional NMR spectra, fitting and simulation results.

References

(1) Sakamoto, R.; Fukui, N.; Maeda, H.; Toyoda, R.; Takaishi, S.; Tanabe, T.; Komeda, J.; Amo-Ochoa, P.; Zamora, F.; Nishihara, H. Layered Metal-Organic Frameworks and Metal-Organic Nanosheets as Functional Materials. *Coord. Chem. Rev.* **2022**, *472*, 214787. https://doi.org/10.1016/j.ccr.2022.214787.

(2) Duan, J.; Li, Y.; Pan, Y.; Behera, N.; Jin, W. Metal-Organic Framework Nanosheets: An Emerging Family of Multifunctional 2D Materials. *Coord. Chem. Rev.* **2019**, *395*, 25–45. https://doi.org/10.1016/j.ccr.2019.05.018.

(3) Guo, L.; Sun, J.; Wei, J.; Liu, Y.; Hou, L.; Yuan, C. Conductive Metal-organic Frameworks: Recent Advances in Electrochemical Energy-related Applications and Perspectives. *Carbon Energy* **2020**, *2* (2), 203–222. https://doi.org/10.1002/cey2.45.

(4) Song, X.; Liu, J.; Zhang, T.; Chen, L. 2D Conductive Metal-Organic Frameworks for Electronics and Spintronics. *Sci. China Chem.* **2020**, *63* (10), 1391–1401. https://doi.org/10.1007/s11426-020-9791-2.

(5) Sheberla, D.; Bachman, J. C.; Elias, J. S.; Sun, C.-J.; Shao-Horn, Y.; Dincă, M. Conductive MOF Electrodes for Stable Supercapacitors with High Areal Capacitance. *Nat. Mater.* **2017**, *16* (2), 220–224. https://doi.org/10.1038/nmat4766.

(6) Campbell, M. G.; Sheberla, D.; Liu, S. F.; Swager, T. M.; Dincă, M. Cu_3 (Hexaiminotriphenylene) $_2$: An Electrically Conductive 2D Metal–Organic Framework for Chemiresistive Sensing. *Angew. Chem. Int. Ed.* **2015**, *54* (14), 4349–4352. https://doi.org/10.1002/anie.201411854.

(7) Grumelli, D.; Wurster, B.; Hötger, D.; Gutzler, R.; Kern, K. Bioinspired Metal Organic Naostructures for Electrcatalysis. *ECS Meet. Abstr.* **2015**, *MA2015-01* (45), 2304–2304. https://doi.org/10.1149/MA2015-01/45/2304.

(8) Fan, Y.; Liu, Z.; Chen, G. Recent Progress in Designing Thermoelectric Metal–Organic Frameworks. *Small* **2021**, *17* (38), 2100505. https://doi.org/10.1002/smll.202100505.

(9) Dolgopolova, E. A.; Rice, A. M.; Martin, C. R.; Shustova, N. B. Photochemistry and Photophysics of MOFs: Steps towards MOF-Based Sensing Enhancements. *Chem. Soc. Rev.* **2018**, *47* (13), 4710–4728. https://doi.org/10.1039/C7CS00861A.

(10) Shin, S.; Gittins, J. W.; Balhatchet, C. J.; Walsh, A.; Forse, A. C. Metal–Organic Framework Supercapacitors: Challenges and Opportunities. *Adv. Funct. Mater.* **2023**, 2308497. https://doi.org/10.1002/adfm.202308497.

(11) Bi, S.; Banda, H.; Chen, M.; Niu, L.; Chen, M.; Wu, T.; Wang, J.; Wang, R.; Feng, J.; Chen, T.; Dincă, M.; Kornyshev, A. A.; Feng, G. Molecular Understanding of Charge Storage and Charging Dynamics in Supercapacitors with MOF Electrodes and Ionic Liquid Electrolytes. *Nat. Mater.* **2020**, *19* (5), 552–558. https://doi.org/10.1038/s41563-019-0598-7.

(12) Shin, S.-J.; Gittins, J. W.; Golomb, M. J.; Forse, A. C.; Walsh, A. Microscopic Origin of Electrochemical Capacitance in Metal–Organic Frameworks. *J. Am. Chem. Soc.* **2023**, *145* (26), 14529–14538. https://doi.org/10.1021/jacs.3c04625.

(13) Gittins, J. W.; Ge, K.; Balhatchet, C. J.; Taberna, P.-L.; Simon, P.; Forse, A. C. Understanding Electrolyte Ion Size Effects on the Performance of Conducting Metal–Organic Framework Supercapacitors. *J. Am. Chem. Soc.* **2024**, *146* (18), 12473–12484. https://doi.org/10.1021/jacs.4c00508.

(14) He, L.; Yang, L.; Dincă, M.; Zhang, R.; Li, J. Observation of Ion Electrosorption in Metal–Organic Framework Micropores with In Operando Small-Angle Neutron Scattering. *Angew. Chem. Int. Ed.* **2020**, *59* (24), 9773–9779. https://doi.org/10.1002/anie.201916201.

(15) Gan, Z.; Wang, Y.; Wang, M.; Gao, E.; Huo, F.; Ding, W.; He, H.; Zhang, S. Ionophobic Nanopores Enhancing the Capacitance and Charging Dynamics in Supercapacitors with Ionic Liquids. *J. Mater. Chem. A* **2021**, *9* (29), 15985–15992. https://doi.org/10.1039/D1TA01818C.

(16) Lian, C.; Liu, H.; Henderson, D.; Wu, J. Can Ionophobic Nanopores Enhance the Energy Storage Capacity of Electric-Double-Layer Capacitors Containing Nonaqueous Electrolytes? *J. Phys. Condens. Matter* **2016**, *28* (41), 414005. https://doi.org/10.1088/0953-8984/28/41/414005.

(17) Kondrat, S.; Kornyshev, A. A. Pressing a Spring: What Does It Take to Maximize the Energy Storage in Nanoporous Supercapacitors? *Nanoscale Horiz.* **2016**, *1* (1), 45–52. https://doi.org/10.1039/C5NH00004A.

(18) Lee, S.-I.; Saito, K.; Kanehashi, K.; Hatakeyama, M.; Mitani, S.; Yoon, S.-H.; Korai, Y.; Mochida, I. 11B NMR Study of the BF 4 - Anion in Activated Carbons at Various Stages of Charge of EDLCs in Organic Electrolyte. *Carbon* **2006**, *44* (12), 2578–2586. https://doi.org/10.1016/j.carbon.2006.06.001.

(19) Forse, A. C.; Griffin, J. M.; Wang, H.; Trease, N. M.; Presser, V.; Gogotsi, Y.; Simon, P.; Grey, C. P. Nuclear Magnetic Resonance Study of Ion Adsorption on Microporous Carbide-Derived Carbon. *Phys. Chem. Chem. Phys.* **2013**, *15* (20), 7722. https://doi.org/10.1039/c3cp51210j.
(20) Forse, A. C.; Griffin, J. M.; Presser, V.; Gogotsi, Y.; Grey, C. P. Ring Current Effects: Factors Affecting the NMR Chemical Shift of Molecules Adsorbed on Porous Carbons. *J. Phys. Chem. C* **2014**, *118* (14), 7508–7514. https://doi.org/10.1021/jp502387x.
(21) Schleyer, P. V. R.; Maerker, C.; Dransfeld, A.; Jiao, H.; Van Eikema Hommes, N. J. R. Nucleus-Independent Chemical Shifts: A Simple and Efficient Aromaticity Probe. *J. Am. Chem. Soc.* **1996**, *118* (26), 6317–6318. https://doi.org/10.1021/ja960582d.
(22) Deschamps, M.; Gilbert, E.; Azais, P.; Raymundo-Piñero, E.; Ammar, M. R.; Simon, P.; Massiot, D.; Béguin, F. Exploring Electrolyte Organization in Supercapacitor Electrodes with Solid-State NMR. *Nat. Mater.* **2013**, *12* (4), 351–358. https://doi.org/10.1038/nmat3567.
(23) Forse, A. C.; Merlet, C.; Griffin, J. M.; Grey, C. P. New Perspectives on the Charging Mechanisms of Supercapacitors. *J. Am. Chem. Soc.* **2016**, *138* (18), 5731–5744. https://doi.org/10.1021/jacs.6b02115.
(24) Fulik, N.; Hippauf, F.; Leistenschneider, D.; Paasch, S.; Kaskel, S.; Brunner, E.; Borchardt, L. Electrolyte Mobility in Supercapacitor Electrodes – Solid State NMR Studies on Hierarchical and Narrow Pore Sized Carbons. *Energy Storage Mater.* **2018**, *12*, 183–190. https://doi.org/10.1016/j.ensm.2017.12.008.
(25) Blanc, F.; Leskes, M.; Grey, C. P. *In Situ* Solid-State NMR Spectroscopy of Electrochemical Cells: Batteries, Supercapacitors, and Fuel Cells. *Acc. Chem. Res.* **2013**, *46* (9), 1952–1963. https://doi.org/10.1021/ar400022u.
(26) Nandy, A.; Forse, A. C.; Witherspoon, V. J.; Reimer, J. A. NMR Spectroscopy Reveals Adsorbate Binding Sites in the Metal–Organic Framework UiO-66(Zr). *J. Phys. Chem. C* **2018**, *122* (15), 8295–8305. https://doi.org/10.1021/acs.jpcc.7b12628.
(27) Bertmer, M. Solid-State NMR of Small Molecule Adsorption in Metal–Organic Frameworks (MOFs). In *Annual Reports on NMR Spectroscopy*; Elsevier, 2020; Vol. 101, pp 1–64. https://doi.org/10.1016/bs.arnmr.2020.07.003.
(28) Klug, C. A.; Swift, M. W.; Miller, J. B.; Lyons, J. L.; Albert, A.; Laskoski, M.; Hangarter, C. M. High Resolution Solid State NMR in Paramagnetic Metal-Organic Frameworks. *Solid State Nucl. Magn. Reson.* **2022**, *120*, 101811. https://doi.org/10.1016/j.ssnmr.2022.101811.
(29) Chen, J. J.; Kong, X.; Sumida, K.; Manumpil, M. A.; Long, J. R.; Reimer, J. A. Ex Situ NMR Relaxometry of Metal–Organic Frameworks for Rapid Surface-Area Screening. *Angew. Chem. Int. Ed.* **2013**, *52* (46), 12043–12046. https://doi.org/10.1002/anie.201305247.
(30) Fricke, S. N.; Salgado, M.; Menezes, T.; Costa Santos, K. M.; Gallagher, N. B.; Song, A.; Wang, J.; Engler, K.; Wang, Y.; Mao, H.; Reimer, J. A. Multivariate Machine Learning Models of Nanoscale Porosity from Ultrafast NMR Relaxometry. *Angew. Chem. Int. Ed.* **2024**, *63* (13), e202316664. https://doi.org/10.1002/anie.202316664.
(31) Chen, S.; Dai, J.; Zeng, X. C. Metal–Organic Kagome Lattices M $_3$ (2,3,6,7,10,11-Hexaiminotriphenylene) $_2$ (M = Ni and Cu): From Semiconducting to Metallic by Metal Substitution. *Phys. Chem. Chem. Phys.* **2015**, *17* (8), 5954–5958. https://doi.org/10.1039/C4CP05328A.
(32) Chen, T.; Dou, J.-H.; Yang, L.; Sun, C.; Libretto, N. J.; Skorupskii, G.; Miller, J. T.; Dincă, M. Continuous Electrical Conductivity Variation in M $_3$ (Hexaiminotriphenylene) $_2$ (M = Co, Ni, Cu) MOF Alloys. *J. Am. Chem. Soc.* **2020**, *142* (28), 12367–12373. https://doi.org/10.1021/jacs.0c04458.
(33) Sheberla, D.; Sun, L.; Blood-Forsythe, M. A.; Er, S.; Wade, C. R.; Brozek, C. K.; Aspuru-Guzik, A.; Dincă, M. High Electrical Conductivity in Ni $_3$ (2,3,6,7,10,11-Hexaiminotriphenylene) $_2$, a Semiconducting Metal–Organic Graphene Analogue. *J. Am. Chem. Soc.* **2014**, *136* (25), 8859–8862. https://doi.org/10.1021/ja502765n.
(34) Zhao, J.; Yuan, H.; Wang, G.; Lim, X. F.; Ye, H.; Wee, V.; Fang, Y.; Lee, J. Y.; Zhao, D. Stabilization of Lithium Metal Anodes by Conductive Metal–Organic Framework Architectures. *J. Mater. Chem. A* **2021**, *9* (20), 12099–12108. https://doi.org/10.1039/D1TA01568K.
(35) Smith, M. K.; Mirica, K. A. Self-Organized Frameworks on Textiles (SOFT): Conductive Fabrics for Simultaneous Sensing, Capture, and Filtration of Gases. *J. Am. Chem. Soc.* **2017**, *139* (46), 16759–16767. https://doi.org/10.1021/jacs.7b08840.
(36) Zhao, W.; Chen, T.; Wang, W.; Jin, B.; Peng, J.; Bi, S.; Jiang, M.; Liu, S.; Zhao, Q.; Huang, W. Conductive Ni3(HITP)2 MOFs Thin Films for Flexible Transparent Supercapacitors with High Rate Capability. *Sci. Bull.* **2020**, *65* (21), 1803–1811. https://doi.org/10.1016/j.scib.2020.06.027.
(37) Wang, L.; Pan, L.; Han, X.; Ha, M. N.; Li, K.; Yu, H.; Zhang, Q.; Li, Y.; Hou, C.; Wang, H. A Portable Ascorbic Acid in Sweat Analysis System Based on Highly Crystalline Conductive Nickel-Based Metal-Organic Framework (Ni-MOF). *J. Colloid Interface Sci.* **2022**, *616*, 326–337. https://doi.org/10.1016/j.jcis.2022.02.058.
(38) Sun, L.; Liao, B.; Sheberla, D.; Kraemer, D.; Zhou, J.; Stach, E. A.; Zakharov, D.; Stavila, V.; Talin, A. A.; Ge, Y.; Allendorf, M. D.; Chen, G.; Léonard, F.; Dincă, M. A Microporous and Naturally Nanostructured Thermoelectric Metal-Organic Framework with Ultralow Thermal Conductivity. *Joule* **2017**, *1* (1), 168–177. https://doi.org/10.1016/j.joule.2017.07.018.
(39) Nazir, A.; Le, H. T. T.; Min, C.-W.; Kasbe, A.; Kim, J.; Jin, C.-S.; Park, C.-J. Coupling of a Conductive Ni $_3$ (2,3,6,7,10,11-Hexaiminotriphenylene) $_2$ Metal–Organic Framework with Silicon Nanoparticles for Use in High-Capacity Lithium-Ion Batteries. *Nanoscale* **2020**, *12* (3), 1629–1642. https://doi.org/10.1039/C9NR08038D.

(40) Lian, Y.; Yang, W.; Zhang, C.; Sun, H.; Deng, Z.; Xu, W.; Song, L.; Ouyang, Z.; Wang, Z.; Guo, J.; Peng, Y. Unpaired 3d Electrons on Atomically Dispersed Cobalt Centres in Coordination Polymers Regulate Both Oxygen Reduction Reaction (ORR) Activity and Selectivity for Use in Zinc–Air Batteries. *Angew. Chem. Int. Ed.* **2020**, *59* (1), 286–294. https://doi.org/10.1002/anie.201910879.
(41) Borysiewicz, M. A.; Dou, J.-H.; Stassen, I.; Dincă, M. Why Conductivity Is Not Always King – Physical Properties Governing the Capacitance of 2D Metal–Organic Framework-Based EDLC Supercapacitor Electrodes: A $Ni_3(HITP)_2$ Case Study. *Faraday Discuss.* **2021**, *231*, 298–304. https://doi.org/10.1039/D1FD00028D.
(42) Cai, D.; Lu, M.; Li, L.; Cao, J.; Chen, D.; Tu, H.; Li, J.; Han, W. A Highly Conductive MOF of Graphene Analogue $Ni_3(HITP)_2$ as a Sulfur Host for High-Performance Lithium–Sulfur Batteries. *Small* **2019**, *15* (44), 1902605. https://doi.org/10.1002/smll.201902605.
(43) Zhang, Z.; Valente, D. S.; Shi, Y.; Limbu, D. K.; Momeni, M. R.; Shakib, F. A. In Silico High-Throughput Design and Prediction of Structural and Electronic Properties of Low-Dimensional Metal–Organic Frameworks. *ACS Appl. Mater. Interfaces* **2023**, *15* (7), 9494–9507. https://doi.org/10.1021/acsami.2c22665.
(44) Nguyen, D. K.; Schepisi, I. M.; Amir, F. Z. Extraordinary Cycling Stability of Ni3(HITP)2 Supercapacitors Fabricated by Electrophoretic Deposition: Cycling at 100,000 Cycles. *Chem. Eng. J.* **2019**, *378*, 122150. https://doi.org/10.1016/j.cej.2019.122150.
(45) Sauerbrey, G. Verwendung von Schwingquarzen zur Wägung dünner Schichten und zur Mikrowägung. *Z. Für Phys.* **1959**, *155* (2), 206–222. https://doi.org/10.1007/BF01337937.
(46) Levi, M. D.; Sigalov, S.; Aurbach, D.; Daikhin, L. In Situ Electrochemical Quartz Crystal Admittance Methodology for Tracking Compositional and Mechanical Changes in Porous Carbon Electrodes. *J. Phys. Chem. C* **2013**, *117* (29), 14876–14889. https://doi.org/10.1021/jp403065y.
(47) Freytag, A. I.; Pauric, A. D.; Krachkovskiy, S. A.; Goward, G. R. In Situ Magic-Angle Spinning ^{7}Li NMR Analysis of a Full Electrochemical Lithium-Ion Battery Using a Jelly Roll Cell Design. *J. Am. Chem. Soc.* **2019**, *141* (35), 13758–13761. https://doi.org/10.1021/jacs.9b06885.
(48) Mohammad, I.; Cambaz, M. A.; Samoson, A.; Fichtner, M.; Witter, R. Development of in Situ High Resolution NMR: Proof-of-Principle for a New (Spinning) Cylindrical Mini-Pellet Approach Applied to a Lithium Ion Battery. *Solid State Nucl. Magn. Reson.* **2024**, *129*, 101914. https://doi.org/10.1016/j.ssnmr.2023.101914.

TOC Graphic